International Journal of Nanoelectronics and Materials
IJNeaM
ISSN 198-5761 | E-ISSN 2232-1535

Physical Investigations of In_2O_3/Porous Silicon at Different Laser Wavelengths

Dua'a R. T. Alrayyes[a], Makram A. Fakhri[a,*], Ali A. Alwahib[a], Motahher A. Qaeed[b] and Subash C.B. Gopinath[c,d,e]

[a]*Laser and Optoelectronic Department, University of technology-Iraq, Baghdad, Iraq.*
[b]*Physics Department, Faculty of Science, University of Jeddah, Jeddah, Saudi Arabia.*
[c]*Institute of Nano Electronic Engineering, Universiti Malaysia Perlis (UniMAP), 01000 Kangar, Perlis, Malaysia.*
[d]*Faculty of Chemical Engineering & Technology, Universiti Malaysia Perlis (UniMAP), 02600 Arau, Perlis, Malaysia.*
[e]*Micro System Technology, Centre of Excellence (CoE), Universiti Malaysia Perlis (UniMAP), Pauh Campus, 02600 Arau, Perlis, Malaysia.*
**Corresponding author. E-mail: mokaram_76@yahoo.com, & makram.a.fakhri@uotechnology.edu.iq*

ABSTRACT

In this study, In_2O_3 thin films deposited on porous silicon using the pulsed laser deposition (PLD) method. The PSi substrate was prepared by photo electrochemical etching with the diode laser assistant. The impacts of various laser wavelengths on structural, spectroscopic, and performance characterizations were investigated. XRD revealed that the In_2O_3/PSi films have a polycrystalline cubic structure. The PL test showed measurements of two emission peaks related to In_2O_3 films (500, 463, 460 nm) and the PSi membrane (857, 852, 829 nm). The peaks at shorter wavelengths increased the energy gap from 2.4 eV to 2.69 eV. AFM results showed the surface roughness of the prepared samples were (3.78, 2.74, 2.3 nm), respectively and the root mean square (4.47, 3.26, 3.12 nm), respectively. FESEM images illustrated that the prepared samples had an average diameter size of (34.51, 25.55, 29.44 nm) with a cauliflower-like shape at 355 nm and rod-shaped particles for both 532 and 1064 nm. EDX tests were performed to figure out the elemental composition of In_2O_3/PSi the concentrations. The longer the laser wavelength, the higher the concentration of indium. The highest laser wavelength increased the transmission while decreasing the absorption.

Keywords: *Indium Oxide, Nanostructure, Nano-films, Photo-electrochemical etching, Porous structure*

1. INTRODUCTION

Indium oxide (In_2O_3) is a semiconductor material that exhibits excellent electrical, optical, and catalytic properties, making it a promising candidate for various applications, including biosensors [1, 2]. In_2O_3's huge surface area, great biocompatibility, and strong conductivity have drawn a lot of interest in biosensor applications [3, 4].

1.1 Characteristics of In_2O_3

A good electrical conductor, In_2O_3 is a translucent, yellow-colored powder with a high electrical conductivity [5, 6]. Its great stability and durability make it a perfect choice for usage in difficult conditions [7, 8]. The huge surface area of in_2O_3 nanoparticles increases their sensitivity to biomolecules, making them a prime option for use in biosensors [9,10].

1.2 Advantages of In_2O_3

Compared to other materials used in biosensors, In_2O_3 offers a number of benefits, including great biocompatibility, strong conductivity, and a high surface area-to-volume ratio [11, 12]. Many techniques, including as co-precipitation, hydrothermal, and sol-gel, may be used to readily manufacture in2o3 [13, 14]. Additionally, In_2O_3 is extremely stable, making it a perfect substance for biosensors that need long-term stability [15, 16].

1.3 Applications of In_2O_3

Biosensors for the detection of several biomolecules, including as glucose, cholesterol, and DNA, frequently employ In_2O_3 [17, 18]. Excellent sensitivity, selectivity, and stability have been reported for In_2O_3-based biosensors, making them perfect for use in clinical and diagnostic applications [19, 20]. Applications for environmental monitoring and food safety have also employed In_2O_3-based biosensors [21, 22].

1.4 Utilization of In_2O_3 in Biosensors

Numerous biosensors, including electrochemical, optical, and field-effect transistor (FET) biosensors, have utilized In_2O_3 [23, 24]. Electrochemical biosensors based on In_2O_3 have been utilized to identify many compounds in blood samples, including glucose, cholesterol, and others [25, 26]. Optical biosensors based on in2O3 have been utilized to find DNA and protein biomarkers in clinical samples [29, 30]. Bacteria and viruses have been found using In_2O_3-based FET biosensors in environmental samples [31, 32].

1.5 Methods of Preparation

Indium oxide may be produced using a variety of techniques, such as chemical vapor deposition, sol-gel, and pulsed laser deposition (PLD). Among these, PLD has drawn a lot of interest because of its capacity to generate

uniform, high-quality thin films with fine control over the deposition settings.

Neodymium-doped yttrium aluminum garnet (Nd:YAG) laser is one of the frequently utilized laser sources for PLD. Utilizing laser pulses of a few nanosecond durations, the Nd:YAG laser PLD approach for indium oxide comprises ablation of an indium oxide target. A thin coating of indium oxide grows after the ablated material is put on a substrate in an oxygen-rich environment.

In order to regulate the structural and optical characteristics of the films, the deposition parameters may be changed, such as the laser fluence, oxygen pressure, and substrate temperature [33, 34].

For instance, a study showed that the indium oxide target's crystalline quality and electrical conductivity were increased by using a high-temperature calcination procedure. [35, 36]. Overall, PLD employing the Nd:YAG laser and other laser sources offers a precise and effective way to create tunable indium oxide thin films, which may be applied in a variety of technical fields [37, 38].

In_2O_3 has good electrical, optical, and catalytic capabilities, making it a suitable material for biosensor applications. Excellent sensitivity, selectivity, and stability of In_2O_3-based biosensors make them the best choice for a variety of applications, including clinical and diagnostic, environmental monitoring, and food safety.

The use of In_2O_3 in a variety of biosensors, such as electrochemical, optical, and FET biosensors, emphasizes the material's potential for use in future biosensor technologies.

2. EXPERIMENTAL WORK

2.1 Preparation of Porous Silicon

Using photo electrochemical etching (PECE), n-type (111) porous silicon samples were created at room temperature. To get rid of any organic impurities, the silicon wafer was carefully cleaned before being chopped into little square pieces. It was inserted into the slot after being put in a Teflon cage with a circular slit at the bottom. This cell contains two electrodes.

The silicon wafer serves as the working electrode, while a counter electrode (usually a platinum wire) and a reference electrode are also included in the cell.

A piece of platinum (Pt) is immersed in an ethanol and hydrofluoric acid (HF) solution at the Teflon cell's top slot, acting as the cathode. The first, which has n-type silicon, functions as an anode and is attached to the bottom of the Teflon cell via an aluminum plate.

The 10% HF and 8% ethanol solution for the conduction of electrons delighted the silicon wafer. In order to construct a nan photonic silicon layer with a current density of 10 mA/cm^2 and an etching duration of 10 min, the illumination source used was a laser diode with a wavelength of 650 nm and a power density of 100 mW/cm^2 (China, TongtoolInc.), DC power supply from 0 to 30V (China, Jiuyuan), Digital multimeter (China, Victor Inc., VC97) and 48% hydrofluoric acid electrolyte solution (Germen, Thomas Baker) and 99.9% ethanol (German, Honeywell Corporation). The laser was positioned 15 cm away from the cell, and platinum was placed at the center of the hole in Teflon's cell. The holes react with the silicon at the surface to create an oxide layer. This oxide layer is then etched away by the HF in the electrolyte solution, as a result of which holes in the silicon form.

The size and shape of the pores can be controlled by adjusting the etching conditions, such as the HF concentration, current density, and illumination intensity. The resulting porous silicon wafer is usually washed with ethanol of 99.9% and dried in an air dryer. It will be illuminated when blue light is shone on it.

2.2 Silicon Substrate

Approximately 1.5 cm x 1.5 cm-sized pieces of the silicon n-type (111) orientation single crystal silicon with (0.02 cm) resistivity and 500 m thickness single side polished wafer samples were split and thoroughly cleaned to remove any contaminants and fingerprints.

2.3 Quartz Substrate

The quartz samples were cut into pieces that were around 1.5 cm by 1.5 cm in size. The quartz material was chosen because it can withstand high temperatures without breaking or being damaged and because, in contrast to other materials, it can accommodate a wide variety of wavelengths.

2.4 Pulsed Laser Deposition (PLD)

Pulsed laser deposition (PLD) is a thin-film deposition technique that utilizes a high-energy pulsed laser to ablate material from a target and deposit it onto a substrate to form a thin film and it is a technique of physical vapor deposition (PVDPLD systems typically include a pulsed laser, vacuum pump, variac, thermometer, and a properly sealed chamber with two pipe-controlled airflow apertures (to avoid any gas leakage). One commonly used laser in PLD is the Nd:YAG (neodymium-doped yttrium aluminum garnet) laser. In the PLD process using an Nd:YAG laser, the laser beam is focused onto the surface of a target material (pressed indium oxide with a thickness of 1.5mm And diameter of 4mm). The target material absorbs the laser energy, causing it to vaporize and form a plasma plume that expands rapidly away from the target surface.

The plasma plume contains a high density of energetic particles, including neutral atoms, ions, and electrons, which are accelerated toward the substrate by the pressure generated by the plume expansion, the PLD parameters are presented in the Table 1. The substrate including pure silicon, porous silicon, and quartz, which is typically placed in close proximity to the target shown in Figure 1, is bombarded by the energetic particles in the

plasma plume, causing the deposition of a thin film. The deposition rate, thickness, and composition of the thin film can be controlled by adjusting the laser energy, pulse duration, and target-substrate distance.

Table 1 The PLD method's practical parameters

Laser Parameters	Values
Laser wavelengths	355nm 532nm 1064nm
The energy of Pulsed	0.9 j
The duration of Pulsed	7 ns
Pulsed Frequency	3 Hz
Power supply	220 V
Repetition rate	300 Hz
Substrate temperature	Porous silicon 300^{O}C

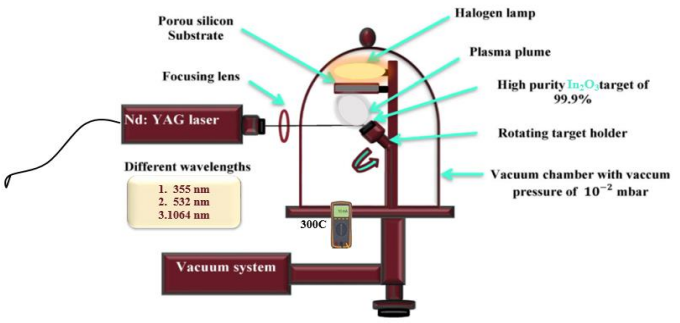

Figure 1. PLD method diagram of n_2O_3 thin film at different laser wavelengths 355, 532, and 1064 nm.

2.5 The Optical Characteristics Using XRD, AFM, FESEM, EDX, PL and UV

The porous silicon was put through several tests in order to find the most effective wavelength for the next step of work. The structural identity was verified by X-ray diffraction (XRD-6000 Shimadzu Co., Japan) of 1.54060 radiations generated by a copper cathode pipe. Field emission scanning electron microscopy (FESEM; Zeiss Co., Germany) was utilized to collect morphological data with high resolution, and photoluminescence (PL; Perkin Elmern Co., USA) was employed to assess the spectroscopic examination. Additionally, topographical structural properties were assessed using atomic force microscopy (AFM; TT2 Co., USA). Furthermore, energy-dispersive X-ray spectroscopy (EDX) was used to determine the elemental composition of a material, and finally, ultraviolet-visible spectroscopy (DR/UV-vis) was employed to measure the absorption and transmission of light in the ultraviolet and visible regions of the electromagnetic spectrum.

3. RESULT AND DISCUSSION

3.1 Crystalline Characteristics (XRD)

Figure 2 displays the PSi substrate with the XRD pattern. Without a diffraction signal at any value higher than 2 = 29^{o}, the pattern was contained in the region of 2 = 27–29. The XRD shows two peaks, one for the silicon at 2θ = 27 ◦ and the other for the PSi adhenished with the silicon at 2θ = 28.02^{o}, related to (200) and (200) planes, respectively. The crystallite size of In_2O_3 can be calculated by using the Scherrer equation [39-41].

$$D = K\lambda / (\beta\cos\theta) \quad (1)$$

where D is the crystallite size, K is Scherrer's constant (usually taken to be 0.9), λ is the wavelength of the X-rays used, β (FWHM) is the full width at half maximum (in Radians) the diffraction peak, and θ is the Bragg angle (half of the diffraction angle) [42-44].

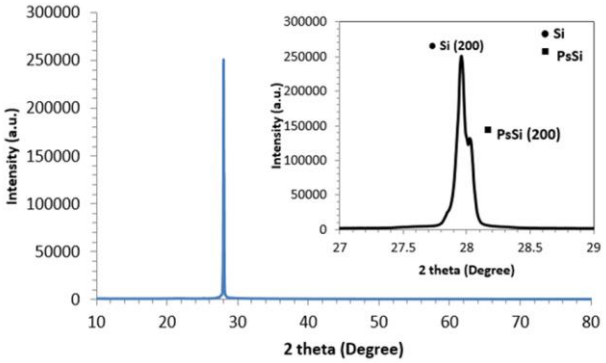

Figure 2. The etching "Photo-electrochemical" assisted by the laser diode aid yielded an XRD pattern of a produced PSi substrate.

The X-Ray Diffraction patterns of In_2O_3 deposited on PSi at various laser wavelengths are shown in Figures 3 (a, b, and c). The position of 2θ in the range of 10^{o}-70^{o}. The XRD patterns revealed that the In_2O_3 films are polycrystalline with a cubic structure [45-47]. All diffraction peaks were listed in Table 2 for each wavelength. The XRD patterns showed peaks in the range of 21 to 60.7, could be attributed to the deposition process of In_2O_3. The most noticeable crystallographic texture was seen in (222), with a high intensity peak in In_2O_3 at 355 nm, where the crystallite size was the smallest at 9.05 nm. The average crystallite size determined by Scherer's equation increased as the laser wavelength became longer.

Table 2 Lists the In_2O_3/PSi XRD properties for various laser wavelengths

Wavelength (nm)	Orientation (hkl)	(2θ) (degree)	FWHM (β) (degree)	The size of the Crystallite (D) (nm)
355	211	21.7	0.31	26.12
	222	30.3	0.91	9.05
	400	35.3	0.61	13.68
	440	50.9	0.11	80.08
	622	60.7	0.19	36.12
532	211	21	0.42	18.62
	222	30.5	0.08	95.93
	400	30.5	0.41	18.71
	440	50.9	0.71	10.11
	622	60.7	0.21	32.68
1064	211	21	0.11	71.10
	222	30.1	0.18	42.67
	400	35	0.59	12.85
	440	50.6	0.15	47.94
	611	58.4	0.55	12.62
	622	60.6	0.19	36.14

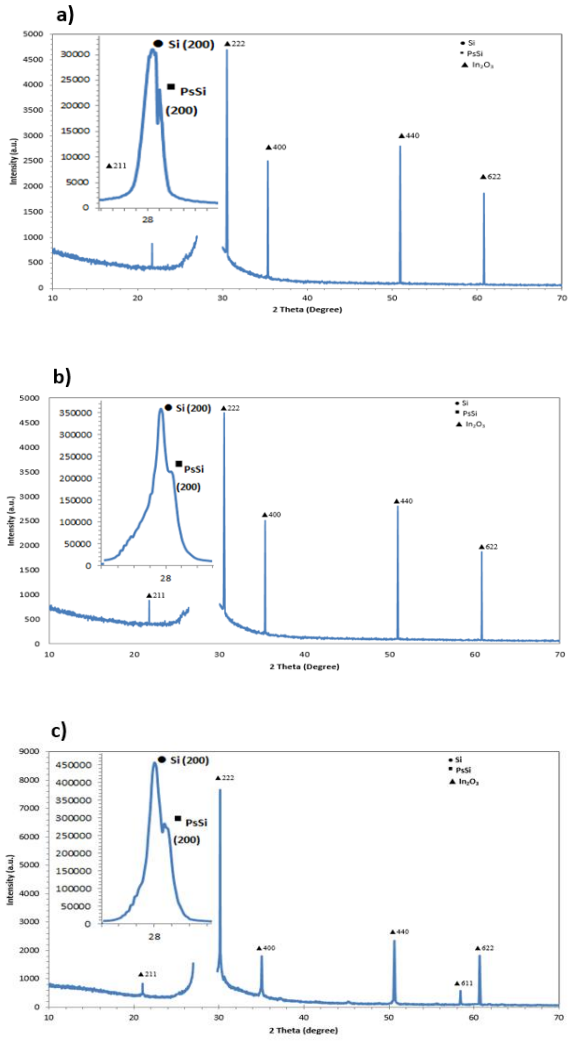

Figure 3. XRD pattern of In_2O_3 a) at 355 nm wavelength, b) at 532 nm wavelength, and c) at 1064 nm wavelength.

3.2 Topographic Results AFM

The surface topography of grown In_2O_3 films was also examined using AFM at various wavelengths, as shown in Figures 4. At 355 nm, the surface was covered in sharp oval particles that formed the In_2O_3 layer. The film's surface roughness was determined to be 3.78 nm, while the surface's root mean square (RMS) was 4.47 nm.

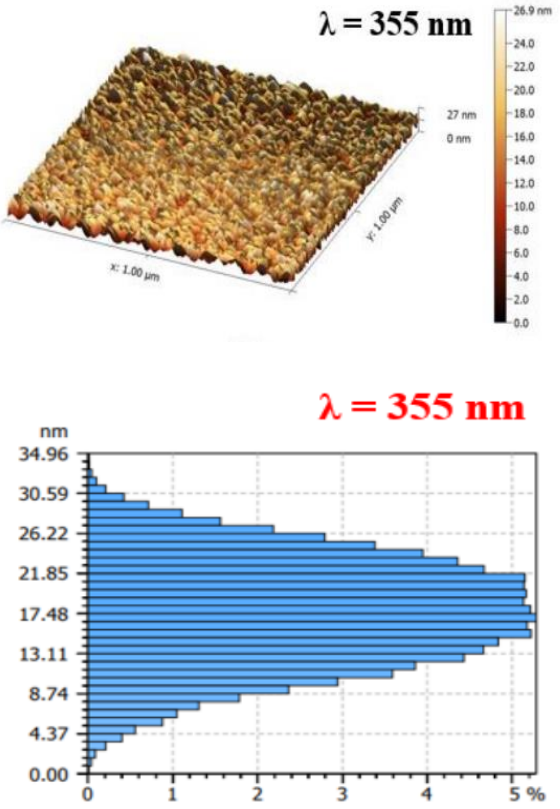

Figure 4. AFM and Histogram of In_2O_3/PSi at different laser wavelengths.

3.3 Surface Morphology FESEM

Figures 5 display FESEM images of In_2O_3 films deposited at 355nm laser wavelengths, the average diameters of the In_2O_3 particles were 34.51 nm. The In_2O_3 film was grown at 355 nm in figure 8 D, and E, and the FESEM photos of the film reveal that it covered the PSi surface with uniform cauliflower-shaped particles with an average diameter of 34.51 nm that grew larger with the shorter wavelength.

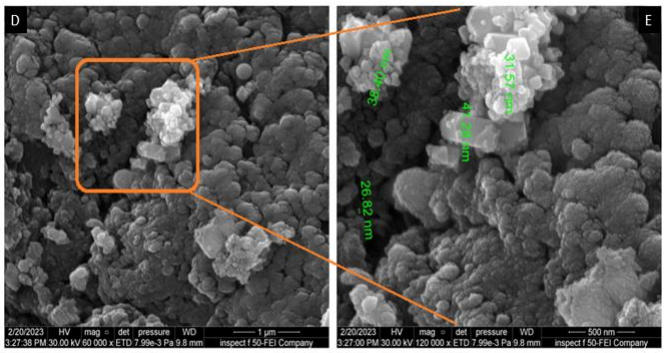

Figure 5. FESEM images of grown In_2O_3 film at wavelength of 355 nm, **D**. Magnified 60,000X, **E**. Magnified 120,000X.

3.4 Energy Dispersive X-ray Spectroscopy (EDX)

Figure 6 illustrated the EDX analysis of the grown In2O3 thin film over Psi. The spectrum displays a prominent silicon peak along with smaller peaks for oxygen and indium, confirming the elemental composition. This analysis verifies the presence of oxygen, silicon, and indium under various laser wavelengths.

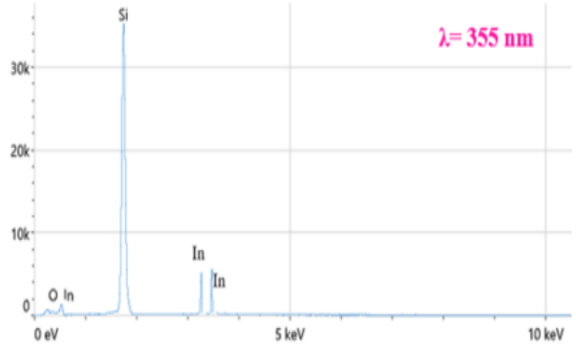

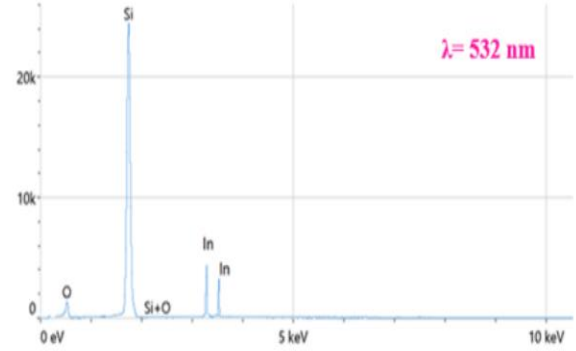

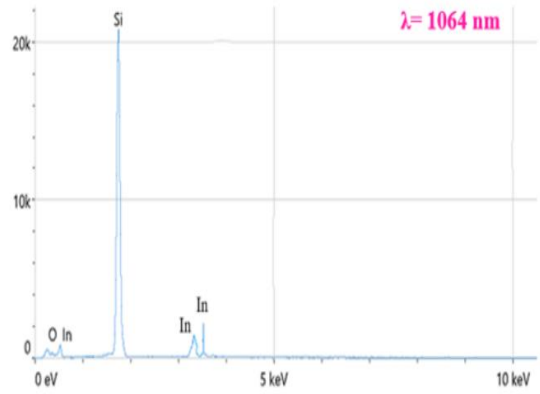

Figure 6. EDX spectrum at different laser wavelengths with 2000 mJ laser energy and 300°C substrate temperature. The X-axis represents counts and the Y-axis (KeV).

3.5 Spectroscopic Properties (Photoluminescence PL)

PL was performed at room temperature. For luminescence, a spectrometer (200-800 nm wavelengths) is used. The energy band gap could be calculated using this equation. [48-50].

$$E_{gap} = hc / \lambda = 1240 / \lambda \text{ (nm)} \quad (2)$$

Where:
E_{gap}: the produced PSi substrate energy band.
h: Planck's constant (6.62×10^{-34} J/Sec)
c: the speed of light (3×10^{8} m/sec)
λ: the wavelength peak of the prepared PSi substrate (847 nm).

Figures 7 show the PL spectra of Nano- In_2O_3 films prepared at 355 laser wavelengths. At 355 nm, the highest PL peak was observed at 500 nm, corresponding to a calculated energy gap of 2.4 eV. This peak was in the UV spectrum, whereas a modest emission peak in the IR spectrum was discovered, which is attributed to the presence of PSi in the sample. The UV peak suggests that the emission is likely due to defects or impurities in the In_2O_3 material rather than direct band-to-band recombination.

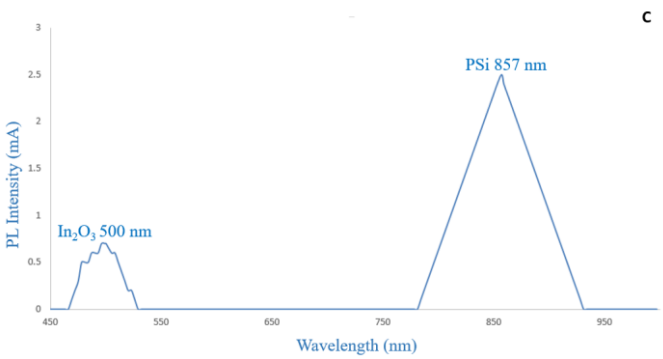

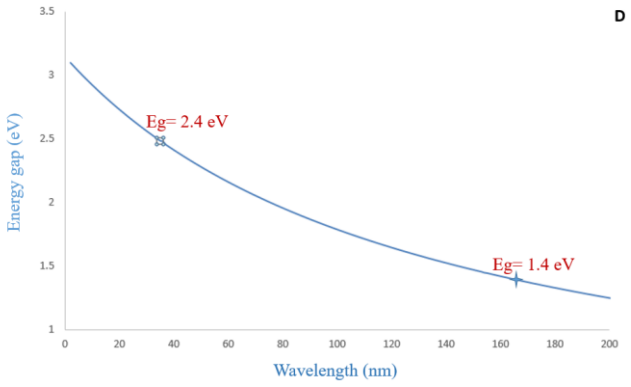

Figure 7. C) Photoluminescence of In_2O_3/PSi at room temperature at 355 nm laser wavelength. D) Energy gap versus wavelength of In_2O_3/PSi at 355 nm laser wavelength.

4. CONCLUSION

In_2O_3 thin films were deposited on a porous silicon substrate by the PLD method. Among the analytical techniques, each serves a specific purpose. The production was performed by the XRD test of In_2O_3 polycrystalline with a cubic structure. We investigated the elemental composition of the In_2O_3 film structures by EDX test. The morphology was tested by AFM and FESEM, which observed a roughness of 2.3 nm and a root mean square of 3.12 nm at 1064 nm, conforming to the best distribution of particles and making it the optimum wavelength.

REFERENCES

[1] R. C. Pawar, S. S. Mali, R. S. Devan, and S. H. Pawar, Materials Science and Engineering: B, vol. 250, pp. 114295, (2020).

[2] M. A. Fakhri, E. T. Salim, S. M. Tariq, R. K. Ibrahim, F. H. Alsultany, A. A. Alwahib, S. F. H. Alhasan, S. C. B. Gopinath, Z. T. Salim & U. Hashim, A gold nanoparticles coated unclad single mode fiber-optic sensor based on localized surface plasmon resonance, Scientific Reports, 13, 5680 (2023). https://doi.org/10.1038/s41598-023-32852-6.

[3] Ismail, R.A., Salim, E.T., Alwazny, M.S., Nanosecond Laser Ablation of Au@LiNbO3 Core–Shell Nanoparticles in Ethanol: Properties and Application in Optoelectronic Devices, Plasmonics, 18(2), pp. 561-576 (2023).

[4] K. H. Kim, Y. K. Kim, K. T. Kim, and J. M. Kim, Nanotechnology, vol. 30, pp. 355101, (2019).

[5] Adam, H., Gopinath, S.C.B., Md Arshad, M.K., ...Sasidharan, S., Wu, Y.S., Integration of microfluidic channel on electrochemical-based nanobiosensors for monoplex and multiplex analyses: An overview, Journal of the Taiwan Institute of Chemical Engineersthis link is disabled, 2023, 146, 104814.

[6] Salim, E.T., Hassan, A.I., Mohamed, F.A., Wahid, M.H.A., Fakhri, M.A., A sight of view on electrical impacts, structural properties and surface roughness of tungsten trioxide thin film: effect of substrate temperatures in WO3/Si device fabrication, Physica Scripta 2023, 98(3), 035508.

[7] Y. Zhang, Y. Zhang, H. Liu, and W. Wang, Al-Ani, Biotechnology Reports, vol. 26, pp. e00422, (2020).

[8] M. A. Fakhri, M. J. A. Razzaq, H. D. Jabbar, E. T. Salim, F. H. Alsultany, U. Hashim, Fabrication of UV photodetector based on GaN/ Psi heterojunction using pulse laser deposition method: Effect of different laser wavelengths, Optical Materialsthis link is disabled, 2023, 137, 113593.

[9] Evan T. Salim, Suhair R. Shafeeq Mohammed Jalal AbdulRazzaq Makram A. Fakhri Subash C. B. Gopinath, Photo-activation of Ag chemicals for enhanced Nb2O5 optoelectronic device employing plasmonic effects, Surfaces and Interfaces, Volume 36, February 2023, 102618.

[10] J. Yan, L. He, X. Cui, Q. Chen, and H. Luo, Journal of Materials Science: Materials in Electronics, vol. 30, no. 19, pp. 17405-17424, (2019).

[11] Fakhri, M. A., Alwahib, A. A., Alhasan, S. F. H., ...Abdulwahab, A. W., Hashim, U., Optoelectronic device based on lithium niobate nanofilms deposited at various pulsed laser wavelengths, Journal of Optics (India) (2023) https://doi.org/10.1007/s12596-023-01173-2.

[12] Osamah, S., Alwahib, A. A., Fakhri, M. A., Gopinath, S.C.B., Study of single and symmetrical D-shaped optical fiber sensor based on gold nanorods, , Journal of Optics (India) (2023)https://doi.org/10.1007/s12596-023-01119-8.

[13] A. S. A. Al-Hadi, S. A. Hussain, S. H. HasanAl-Ani, Biotechnology Reports, vol. 26, pp. e00422, (2020).

[14] Hassan, N. K., Khalid, F. G., Ekshayesh, A. A., ...Dahham, O. S., Hussein, M. M., Optical investigations of gold nano rods and gold nano rods doped with ZnO nanoparticles for optoelectronic applications, Journal of Optics (India) (2023) https://doi.org/10.1007/s12596-023-01120-1.

[15] Salim, E. T., Saimon, J. A., Abood, M. K., ...Alsultany, F.H., A Preliminary Study on Structural and Optical Properties of Heat Treated Nb2O5 Nanostructure, International Journal of Nanoelectronics and Materials, 16(1), pp. 21-32 (2023).

[16] S. Iqbal, M. A. B. S. Shah, M. M. Qamar, and M. R. Khan, Journal of Materials Science: Materials in Electronics, vol. 31, no. 3, pp. 1413-1428, (2020).

[17] Haneen D. Jabbar Makram A. Fakhri, Mohammed Jalal Abdul Razzaq, Omar S. Dahham, Evan T. Salim, Forat H. Alsultany, Effect of Different Etching Time on Fabrication of an Optoelectronic Device Based on GaN/Psi, Journal of Renewable Materials 2023, 11(3), 1101-1122. https://doi.org/10.32604/jrm.2023.023698.

[18] Sara M. Tariq, and Makram A. Fakhri, Design and Simulation of Optical Fibre Based of Gold Nanoparticles for Sensor Applications, International Journal of Nanoelectronics and Materials Volume 15 (Special Issue) December 2022 [59-70].

[19] S. P. Singh, P. Pandey, A. Kumar, and V. K. Singh, Journal of Sol-Gel Science and Technology, vol. 93, no. 1, pp. 1-19, (2020).

[20] Malik J. Abd-ALhussain, Bassam G. Rasheed, and Makram A. Fakhri, Review on Photonic Crystal Fiber-Based Nanoparticle for Sensing Applications, International Journal of Nanoelectronics and Materials Volume 15 (Special Issue) December 2022 [71-79].

[21] Rami S. Mohammed, Makram A. Fakhri, Forat H. Alsultany, and U. Hashim, Synthesis of Titanium-Dioxide using Pulsed Laser Deposition at Various Pulsed Laser Energies, International Journal of Nanoelectronics and Materials Volume 15 (Special Issue) December 2022 [93-102].

[22] J. Kim, H. Lee, J. Park, and J. H. Lee, ACS Applied Materials and Interfaces, vol. 12, no. 17, pp. 19825-19832, (2020).

[23] Reem M. Khalaf, and Makram A. Fakhri, Structural and Morphological Investigations of Indium Trioxide Deposited using PLD at Different Pulsed Laser Energies, International Journal of Nanoelectronics and Materials Volume 15 (Special Issue) December 2022 [103-110].

[24] Deyhaa A. Resen, Mohammed F. Mohammed, and Makram A. Fakhri, Review of Recent Optical Bio-Sensor Based FBG, International Journal of Nanoelectronics and Materials Volume 15 (Special Issue) December 2022 [165-181].

[25] S. Palanisamy, S. Thanikaivelan, and S. Ponnusamy, in Nanobiosensors, Elsevier, (2020), pp. 139-150.

[26] Suhair R. Shafeeq, Evan T. Salim, and Mohammed Jalal AbdulRazzaq, Niobium Pentoxide Nanostructures Fabricated by the Fundamental QSwitched Nd:YAG PLD under Vacuum Conditions, International Journal of Nanoelectronics and Materials Volume 15 (Special Issue) December 2022 [1-12].

[27] Tamara E. Abdulrahman, Rana O. Mahdi, and Evan T. Salim, Synthesis of Nb2O5 Nanoparticle by Liquid Phase Laser Ablation Method, International Journal of Nanoelectronics and Materials Volume 15 (Special Issue) December 2022 [13-25].

[28] N. Barfidokht, M. Z. Hassan, F. Ahmad, and M. H. Yaacob, Journal of Materials Science: Materials in Electronics, vol. 31, no. 6, pp. 3752-3774, (2020).

[29] Rawan Bashar Fadhil, Evan T. Salim, Wafaa. K. Khalef, and Forat H. Alsultany, Deposition Time Effect on LN Films Properties Using Chemical Bath Deposition Method without Post Heat Treatment, International Journal of Nanoelectronics and Materials Volume 15 (Special Issue) December 2022 [49-58].

[30] H. Song, H. J. Joo, S. Yoon, and S. W. Han, Biosensors and Bioelectronics, vol. 169, pp. 112574, (2020).

[31] Maryam S. Muhsin, Jehan A. Saimon, and Evan T. Salim, Incorporation of Metal Nanoparticle to Enhance Tungsten Oxide (WO3) Films Properties: A Mini Review, International Journal of Nanoelectronics and Materials Volume 15 (Special Issue) December 2022 [111-118].

[32] Azzam Y. Kudhur, Evan T. Salim, Ilker Kara, Rana O. Mahdi, and Forat H. Alsultany, Applications of Cu2O Nanoparticles Prepared via Various Techniques: A Review Paper, International Journal of Nanoelectronics and Materials Volume 15 (Special Issue) December 2022 [131-137].

[33] Y. Zhang, X. Xu, Z. Wei, H. Zhang, and J. Liu, Materials Today Chemistry, vol. 17, pp. 100326, (2020).

[34] Fakhri, M. A., Mohammed, R.S., Preparation and characterization of titanium dioxide using PLD at various energy of pulsed laser, Advances in Natural Sciences: Nanoscience and Nanotechnology, 13(4), 045013 (2022). DOI 10.1088/2043-6262/aca60a.

[35] H. D. abbar, M. A. Fakhri, M. J. AbdulRazzaq, Synthesis Gallium Nitride on Porous Silicon Nano-Structure for Optoelectronics Devices. Silicon 14(18), 12837-12853 (2022). https://doi.org/10.1007/s12633-022-01999-8.

[36] S. Shinde, S. R. Sangle, S. S. Mali, and S. H. Pawar, Biosensors and Bioelectronics, vol. 176, pp. 112915, (2021).

[37] F. A. Mohamed, E. T. Salim, A. I. Hassan, Monoclinic tungsten trioxide (WO3) thin films using spraying pyrolysis: electrical, structural and stoichiometric ratio at different molarity, Digest Journal of Nanomaterials and Biostructures 17(3), 1029 – 1043 (2022).

[38] Rawan B Fafhil, Evan T. Salim, Wafaa. K. Khalef, Synthesis of LiNbO3 microstructures: structural, optical, and surface morphology using Chemical bath deposition (CBD) method without post-heat treatment, Egyptian Journal of Chemistry, 66(4), 63-70 2023, 10.21608/EJCHEM.2022.129669.5749.

[39] K. V. Chaitanya, K. Naveen Kumar, K. D. Kadam, and K. M. K. Swamy, Journal of Materials Science: Materials in Electronics, vol. 32, no. 3, pp. 2435-2446, (2021).

[40] Tamara E Abdulrahman, Evan T Salim, Rana O Mahdi and MHA Wahid, Nb2O5 nano and microspheres fabricated by laser ablation, 2022 Adv. Nat. Sci: Nanosci. Nanotechnol. 13 045006 DOI 10.1088/2043-6262/ac99cf.

[41] Evan T. Salim, Ayat Mohammed Yahya, and Ahmed. W. Abdulwahab, Opto-electronic behavior of LN as a dielectric films: Improved using low temperatures treatment, AIP Conference Proceedings 2660, 020130 (2022); https://doi.org/10.1063/5.0107748.

[42] C. Hu, Y. Liu, and Y. Li, Biosensors and Bioelectronics, vol. 171, pp. 112703, (2021).

[43] Fakhri M.A., Jabbar H.D., Alsultany F.H., Salim E.T., Hashim U., Lithium Niobate -Based Sensors: A review, AIP Conference Proceedings 2660, 020124 (2022); https://doi.org/10.1063/5.0107759.

[44] Rami S. Mohammed and Makram A. Fakhri, Titanium Dioxide -Based Sensors: A review, AIP Conference Proceedings, 2660, 020133 (2022); https://doi.org/10.1063/5.0107767.

[45] J. Shao, Z. Huang, Q. Wang, and H. Liu, Journal of Physics: Conference Series, vol. 1333, no. 1, p. 012007, (2019).

[46] Makram A Fakhri, Ali A Alwahib, Evan T Salim, Husam Aldin A Abdul Amir, Forat H Alsultany and U Hashim, Synthesis and characterization of GaN/quartz nanostructure using pulsed laser ablation in liquid Published 19 October 2022 • © 2022 IOP Publishing Ltd.

[47] Physica Scripta, Volume 97, Number 11 115813 DOI 10.1088/1402-4896/ac9866.

[48] H. A. A. A. Amir, M. A.Fakhri, A. A. Alwahib, E. T. Salim, F. H. Alsultany, U. Hashim, Synthesis of gallium nitride nanostructure using pulsed laser ablation in liquid for photoelectric detector, Materials Science in Semiconductor Processing, 150 (2022) 106911.

[49] H. K. Varma, S. K. Mehta, P. S. Patil, S. B. Kondawar, and S. K. Dhopte, Journal of Alloys and Compounds, vol. 775, pp. 1018-1026, (2019).

[50] Evan T. Salim, Ali A. Taha, Sura A. Abdullatef, and Mohammed M. Farhan, Anti-microbial and anti-tumor activity of niobium oxide nano powder, AIP Conference Proceedings 2400, 030015 (2022); https://doi.org/10.1063/5.0112133.

[51] 50) Suhair R Shafeeq, Mohammed Jalal Abdul Razzaq, Evan T Salim, Mohammed HA Wahid, Significance of Niobium (V) Oxide for Practical Applications: A Review, Key Engineering Materials, 911, (2022) 89-95.